



## OPEN Deciphering metabolomics and lipidomics landscape in zebrafish hypertrophic cardiomyopathy model

Shana Jacob<sup>1</sup>, Tala Abuarja<sup>1</sup>, Rulan Shaath<sup>1,2</sup>, Waseem Hasan<sup>1</sup>, Saroja Balayya<sup>1</sup>, Doua Abdelrahman<sup>1</sup>, Khalid Almana<sup>3</sup>, Hajira Afreen<sup>4</sup>, Ahmad Hani<sup>1</sup>, Michail Nomikos<sup>5</sup>, Khalid Fakhro<sup>1,2,6</sup>, Mohamed A. Elrayess<sup>5,7</sup> & Sahar Isa Da'as<sup>1,2</sup>✉

To elucidate the lipidomic and metabolomic alterations associated with hypertrophic cardiomyopathy (HCM) pathogenesis, we utilized *cmybpc3*<sup>-/-</sup> zebrafish model. Fatty acid profiling revealed variability of 10 fatty acids profiles, with heterozygous (HT) and homozygous (HM) groups exhibiting distinct patterns. Hierarchical cluster analysis and multivariate analyses demonstrated a clear separation of HM from HT and control (CO) groups related to cardiac remodeling. Lipidomic profiling identified 257 annotated lipids, with two significantly dysregulated between CO and HT, and 59 between HM and CO. Acylcarnitines and phosphatidylcholines were identified as key contributors to group differentiation, suggesting a shift in energy source. Untargeted metabolomics revealed 110 and 53 significantly dysregulated metabolites. Pathway enrichment analysis highlighted perturbations in multiple metabolic pathways in the HM group, including nicotinate, nicotinamide, purine, glyoxylate, dicarboxylate, glycerophospholipid, pyrimidine, and amino acid metabolism. Our study provides comprehensive insights into the lipidomic and metabolomic unique signatures associated with *cmybpc3*<sup>-/-</sup> induced HCM in zebrafish. The identified biomarkers and dysregulated pathways shed light on the metabolic perturbations underlying HCM pathology, offering potential targets for further investigation and potential new therapeutic interventions.

**Keywords** Hypertrophic cardiomyopathy, Lipidomics, Metabolomics, MYBPC3, Zebrafish

Hypertrophic Cardiomyopathy (HCM) is a disorder with an estimated prevalence of 1 in 500, clinically characterized by left ventricular myocardial wall hypertrophy in the absence of other systemic, metabolic, or cardiac diseases<sup>1–3</sup>. It has a critical complication of sudden death due to cardiac failure<sup>4</sup>, especially in asymptomatic athletes and younger patients<sup>5</sup>. HCM is a heterogeneous disease caused by pathogenic variation in genes encoding sarcomeric, Z-disc, and calcium-controlling proteins<sup>1</sup>. The most prevalent genetic variants impact sarcomeric-encoding proteins (40–60%), affecting the contractility of the heart. These include myosin heavy chain 7 (MYH7), myosin binding protein C3 (MYBPC3), cardiac troponin T2 (TNNT2) and cardiac troponin I3 (TNNI3)<sup>6–9</sup>.

With a frequency of ~30–40%, pathogenic variants in *MYBPC3* are the most common cause of HCM<sup>10,11</sup>. This is attributed to its vital role in sarcomeric structural configuration and function through modulation of myofilament sliding velocity and its key contribution to the actin-myosin interaction, which is responsible for contractility<sup>12,13</sup>. Pathogenic *MYBPC3* variants are typically frameshift, non-sense, or splice site variants, which lead to premature termination codons (PTC)<sup>14</sup>. Consequently, PTCs are degraded through non-sense mediated RNA decay, which could lead to allelic loss of function, impacting the function of the protein and interaction with other associated proteins<sup>12,15</sup>.

Despite the significant contribution of genetic variants in understanding the etiology of HCM, they have been proven insufficient in fully capturing the overall associated clinical and pathological features related to

<sup>1</sup>Research Department, Sidra Medicine, Doha 26999, Qatar. <sup>2</sup>College of Health and Life Sciences, Hamad Bin Khalifa University, Doha 34110, Qatar. <sup>3</sup>Department of Biochemistry, Swansea University, SA1 8EN Swansea, UK. <sup>4</sup>Department of Biological Sciences, Qatar University, Doha 2713, Qatar. <sup>5</sup>College of Medicine, QU Health, Qatar University, Doha 2713, Qatar. <sup>6</sup>Weill Cornell Medical College, Doha 24144, Qatar. <sup>7</sup>Biomedical Research Center, Qatar University, Doha 2713, Qatar. ✉email: sdaas@sidra.org

clinical presentations and severity<sup>16</sup>. Thus, the clinical picture of ~40% of HCM patients remains unresolved when assessed through clinical examination and genetic testing<sup>17,18</sup>.

Changes in cardiac structure and function in HCM often correlate with changes in energy consumption as a compensation mechanism in HCM<sup>19</sup>. In the heart, ATP is the primary source of energy and adaptation to energy demands throughout the day due to physiological and nutritional changes is crucial. ATP can be sourced from metabolites including amino acids, lipids, and carbohydrates. Disturbances in ATP supply could thus lead to alterations in cardiac activity and eventual cardiovascular diseases (CVDs)<sup>20</sup>. Cellular studies have depicted that HCM-associated variants increase the demand for utilizing ATP, thus emphasizing a higher requirement for myocardial energy in HCM patients<sup>4</sup>. As there is insufficient ATPase activity in such patients, it is hypothesized that the higher demand for energy leads to energy stress and adverse remodeling within the heart<sup>4</sup>. Thus, understanding the changes in cardiac metabolic activity could provide an avenue for further understanding of CVDs, including HCM. Through the integration of metabolomics and lipidomics profiling, the identification of distinct metabolite features and changes associated with a genotype, environmental factors, including diet and physical activity could lead to a wider understanding of HCM etiology.

The zebrafish model has been reported to possess a similar metabolism to humans<sup>21</sup>, making it an increasingly common target for metabolomic studies<sup>22</sup>. Zebrafish *cmybpc3* knockout line has been previously employed and proven as an efficient model to study the association of genetic variants and clinical presentation<sup>23–25</sup>.

To shed more light on the relationship between metabolic activity and HCM, with the aim to improve diagnosis efficiency and patient stratification, lipidomics, metabolomics, and fatty acid signatures, analysis of heterozygous and homozygous established zebrafish MYBPC3-HCM models is performed. The ultimate goal is to tackle the pathophysiological interactions of biomarkers related to HCM progression.

## Results

### Sample collection

We analyzed 21 zebrafish homogenate samples through lipidomics and metabolomics to study HCM signatures in order to identify, relatively quantify, and statistically compare lipids and metabolites between the experimental groups of transgenic reporter Tg myl7:eGFP line as a control (CO), *cmybpc3*<sup>+/-</sup>::myl7:eGFP heterozygous (HT), and *cmybpc3*<sup>-/-</sup>::myl7:eGFP homozygous (HM) (Fig. 1) using liquid chromatography-high resolution mass spectrometry. In total, we have analyzed 7 replicates for each group of CO, HT and HM; each replicate included pooled 150 larvae. Each sample's performance was monitored with the addition of isotopically labeled internal standards through analysis. These internal standards were monitored for mass accuracy, peak area response, and retention time variability. All parameters were within accepted criteria of 3ppm, +/- 30% of the median and +/- 2% of the median, respectively. The selection of features for analysis was designed to capture the metabolic and lipidomic alterations associated with HCM. Diverse data sources, including an in-house MS2 library and mzCloud for metabolomics and LipidSearch for lipidomics, were incorporated to provide wide coverage of potential biomarkers and metabolic pathways.

Fatty acids, acylcarnitines and lipidomic changes associated with *cmybpc3*-HCM zebrafish model.

A total of 10 fatty acids were detected in the zebrafish lysate that showed variability in fatty acids profile between the different groups. Hierarchical cluster analysis revealed that both HT and HM groups showed variability in concentrations of detected fatty acids (Fig. 2).

PCA showed the clustering of the three examined groups with the first two principal components explaining 81.8% of the variability. The HM group showed a relatively distinct separation in comparison to the CO and HT groups, despite the 95% confidence region overlapping between HM and the other groups (Fig. 3A).

The PLS-DA differentiated metabolic phenotypes with the first component explaining 67.5% of the variability (Supplementary Figure S1). The results highlight 9,12,15-octadecatrienoic acid as the variable showing the highest VIP score of 1.95 for component 1, followed by hexadecanoic acid (Supplementary Figure S1). Particularly, 13-Octadecanoic acid (C18:1), 9,12-Octadecadienoic acid, 9,12,15-octadecatrienoic acid, Hexadecanoic acid, 14-methyl-, and 5,8,11,14,17-Eicosapentaenoic acid, were significant between the control group (CO) and *cmybpc3*<sup>-/-</sup> homozygous group (HM) (Supplementary Figure S1).

We analyzed the total lipids to identify lipidomic profiling to relate key lipid biomarkers in the *cmybpc3*-HCM model. Lipid profiling determined a total of 221 lipid annotations where fragmentation spectra were matched against LipidSearch software (Supplementary Table S1). The annotated lipid compounds covered several lipid classes: acylcarnitines, carnitine esters, ceramides, diacylglycerols, hexosylceramides, lysophosphatidylcholines, lysophosphatidylethanolamines, phosphatidylcholines, phosphatidylethanolamines, phosphatidylglycerol phosphatidylinositol, phosphatidylmethanol, sphingomyelin, triacylglycerol and coenzyme-Q10. A total of two lipids were significantly dysregulated between the CO and HT; and 48 lipids between CO and HM groups using One way ANOVA analysis with Tukey as post-hoc test (Supplementary Table S2 and S3) with false discovery rate (FDR) < 0.05. The first two principal components explained 54.3% of the variability in *cmybpc3*-HCM models (Fig. 3B).

Sparse Partial Least Squares-Discriminant Analysis (sPLS-DA) using five components with 10 variables per component established a clear separation between the three groups based on lipidomic profiles (Supplementary Figure S2). The results demonstrate that acylcarnitines and phosphatidylcholines contribute the most to the differentiation between the three examined groups (Supplementary Figure S2). The results of the hierarchical clustering indicated that within the homozygous group, there is observed variability in the concentrations of lipids that form a distinct signature in the mutant HCM model (Supplementary Figure S2).

To discriminate between the three groups, we compared the groups using acylcarnitines profiles. The first two components, acylcarnitines (18:3 and 20:4), explained 88.2% of this variability between CO, HT and HM samples. The HM samples clustered separately from the CO, HT groups (Fig. 3C). The hierarchical cluster analysis

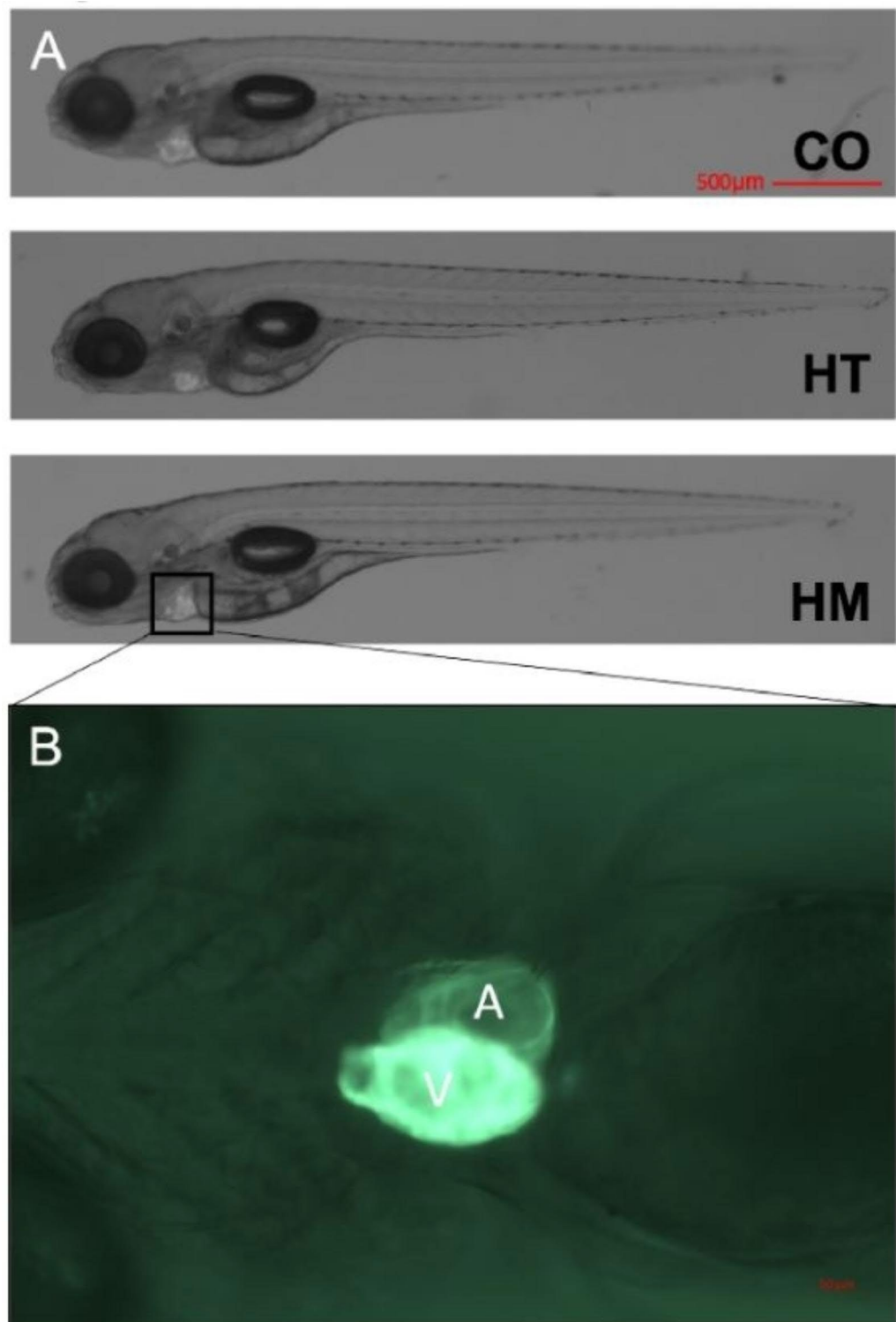


**Fig. 1.** Representative images of the zebrafish larvae at 5 days old. **(A)** Representative lateral view of zebrafish larvae (control (CO), *cmybpc3*<sup>+/-</sup>::*myl7:eGFP* heterozygous (HT), and *cmybpc3*<sup>-/-</sup>::*myl7:eGFP* homozygous (HM)) Transgenic reporter line *myl7:egfp* expressing green fluorescent two-chambered heart (500 μm scale bar). **(B)** A ventral view of HM heart at 168x high-magnification image captured using Axiozoom Zeiss stereomicroscope equipped with Axioacam camera, scale bar 50 μm.

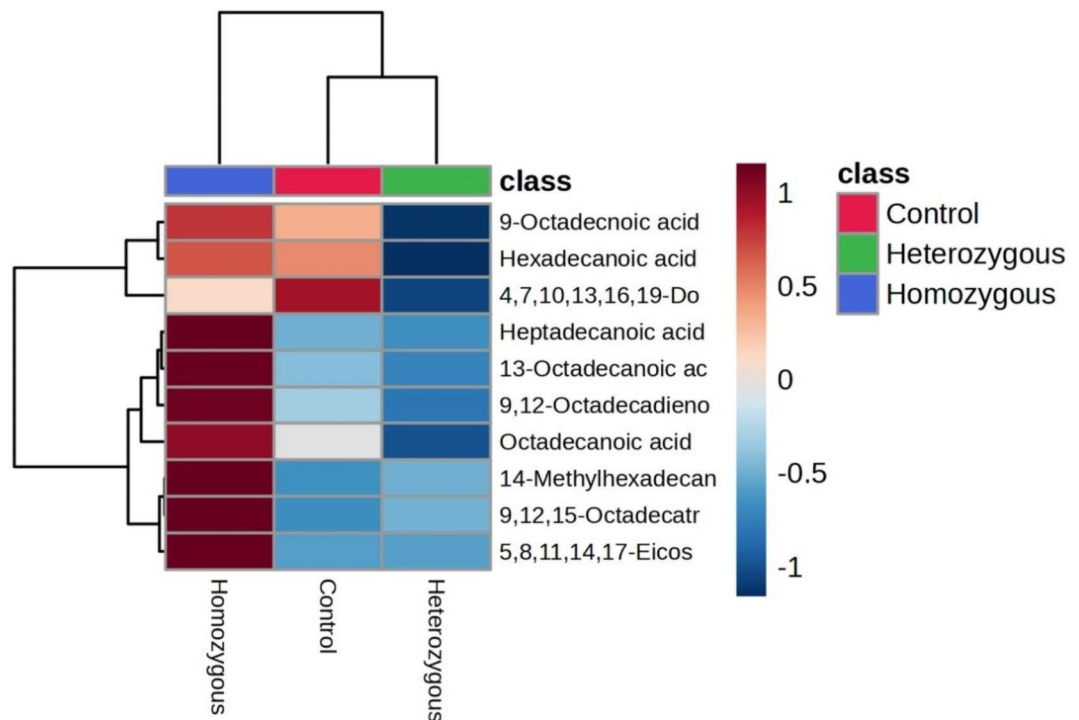


**Fig. 2.** Hierarchical cluster analysis of fatty acids. Z-score clustering results for fatty acids are shown as a heatmap for all samples using MetaboAnalyst 5.0. The distance measure was Euclidean, and clustering method was Ward. The rows and columns are ordered so that similar groups and similar metabolites are close to one another. The fatty acids are present in the rows, and the sample groups in columns. Dark blue to dark red color gradient denotes lower to higher levels. On the top of the heatmap, the homozygous sample group is represented in blue, the heterozygous group in green and the control group in red.

demonstrated that the HM group clusters separately with an elevation in acylcarnitine levels (Supplementary Figure S3).

The PLS-DA model revealed significant discrimination in the metabolic phenotypes of acylcarnitines. The acylcarnitines with the highest VIP scores, contributing to the differentiation of the HM group from the other HT and CO groups, were highlighted in Supplementary Figure S3B and S3C.

To understand the underlying metabolic perturbation of *cmybc3*<sup>-/-</sup> related pathological HCM, untargeted metabolomics was employed to characterize the differences between the examined groups. A total of 110 and 53 metabolites were annotated under positive and negative ESI modes, respectively with an MS2 fragmentation pattern match in an in-house library or mzCloud software (Supplementary Table S4). A total of 13 metabolites were significantly dysregulated between HM and CO (Supplementary Table S5), while none were significant between HT and CO, with FDR < 0.05.

PCA did not show clear clustering between the groups with the first two components explaining 48.4% of the variability (Fig. 3D). Further analysis using sPLS-DA with 10 variables per component on the top 5 components showed a more distinct separation of the HM samples and a unique metabolic signature related to both HM and HT groups (Supplementary Figure S4).

To explore the significant metabolites distinguishing HCM phenotype, we compared between two groups: HM and CO groups, HM and HT groups, HT and CO groups. Metabolites were considered significant if they had a log<sub>2</sub> fold change > 1 and FDR < 0.05. Comparing HM and CO groups, among the 163 identified metabolites, 16 were significant, with 6 showing downregulation and 10 upregulation (Supplementary Figure S4). The OPLS-DA revealed a clear and distinct clustering of the HM and CO groups with R<sup>2</sup>Y (model interpretation rate) of 87.7% and Q<sup>2</sup> (model predictive ability) of 74.5% (Supplementary Figure S4). Metabolites with VIP > 1 were selected as important metabolites with asparagine showing the highest VIP score, followed by stachydrine (Supplementary Figure S4). Furthermore, Random Forest model demonstrates robust discriminatory power with AUROC curve (Area Under the Receiver Operating Characteristic curve) of 0.995 (CI 1–1) using 15 features (Fig. 4A) and predictive accuracy of 93%. The metabolites were mapped to pathways to determine pathways enriched in the HM group compared to CO group. The enrichment analysis shows that 8 pathways were significantly dysregulated with FDR < 0.05 (Fig. 5A and Supplementary Table S6).

The pathways involved the metabolism of nicotinate, nicotinamide, purine, glyoxylate, dicarboxylate, glycerophospholipid, pyrimidine, pantothenate, CoA, sphingolipid, alanine, aspartate, and glutamate metabolism. Comparing HM to HT group, 26 metabolites displayed significantly different levels, 24 upregulated and 2 downregulated (Supplementary Figure S4). The Random Forest model effectively differentiates between these groups with AUROC of 1 (1–1) using 10 features (Fig. 4B) and a predictive accuracy of 98%. Pathway

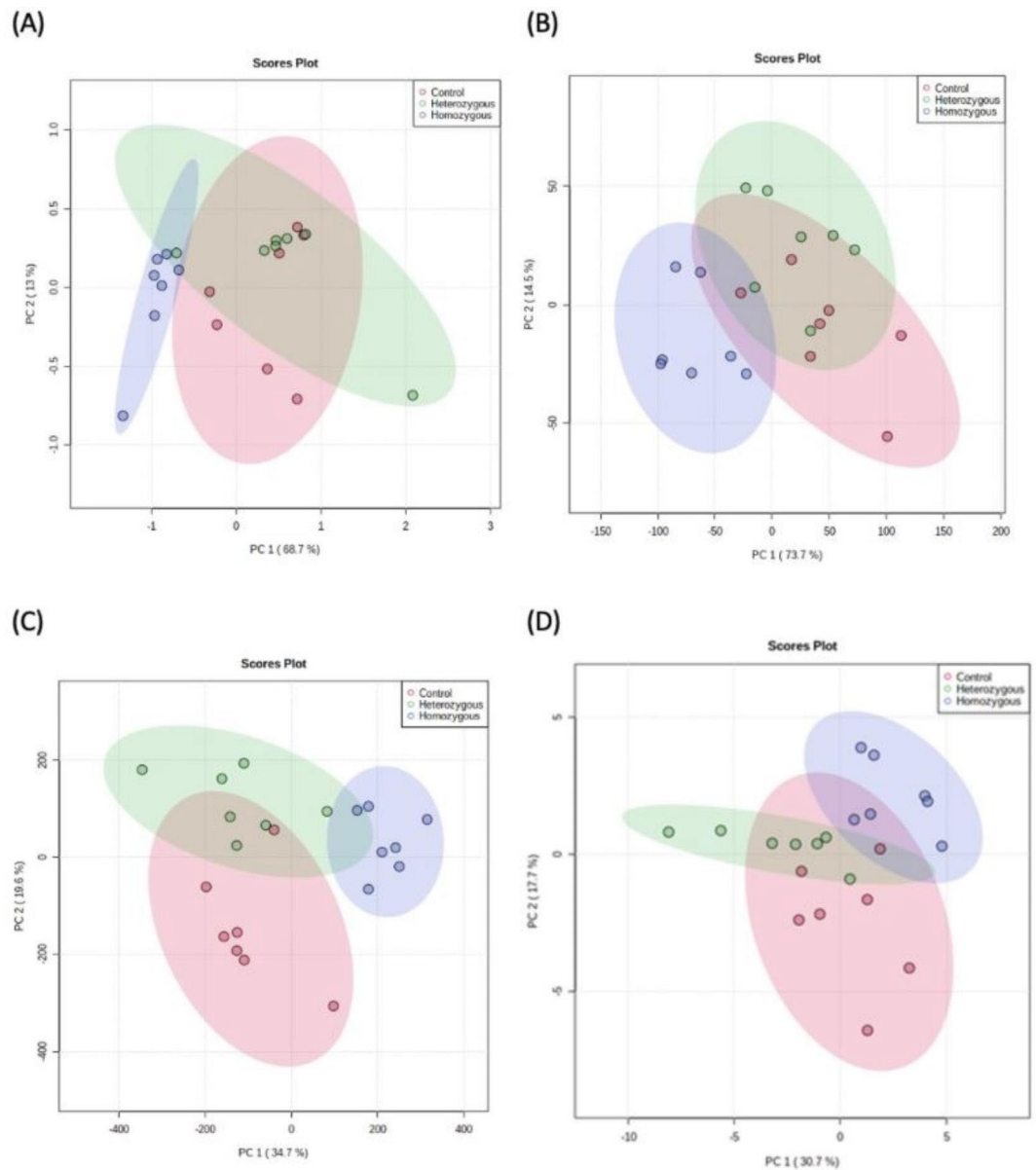


**Fig. 3.** Principal components analysis (PCA) graph. The percentages on the axes represent the variation in the data set of the first two components. The points in the shaded regions represent the 95% confidence interval of each group and any overlaps between groups. The PCAs were generated using MetaboAnalyst 5.0 comparing between sample groups (control (CO), *cmybpc3*<sup>+/-</sup>::*myl7*:eGFP heterozygous (HT), and *cmybpc3*<sup>-/-</sup>::*myl7*:eGFP homozygous (HM)). **(A)** Fatty Acids, **(B)** Acycarnitines, **(C)** Lipids and **(D)** Metabolites.

enrichment analysis revealed significant pathways involving cysteine, methionine, nicotinate, nicotinamide, phenylalanine, tyrosine, and tryptophan metabolism (Fig. 5B and Supplementary Table S7). Comparison between HT and CO groups revealed that only 3 metabolites showed significantly different levels of nicotinic acid, ornithine, and prolinamide. Between these two groups, no pathways were highlighted with an FDR < 0.05.

## Discussion

There is limited research on HCM metabolic alterations in cardiac remodeling. Herein, we performed a comprehensive multi-omics assessment at the early stages of cardiac remodeling in HCM utilizing the zebrafish model. Our integrative omics analysis reveals unique metabolic and lipidomic alterations implying the impact on critical molecular and biochemical pathways contributing to HCM pathophysiology. We collected 150 larvae in 7 replicates of *cmybpc3* HCM zebrafish model at 5 days post-fertilization (dpf), as the heart is fully developed by 3dpf. In the zebrafish, at 1dpf, the heart is a valveless tube, at 1.5dpf cardiac looping and chamber ballooning occur, followed by the formation of the two-chamber heart at 2dpf, and finally at 3dpf ventricular trabeculation occurs<sup>26</sup>.

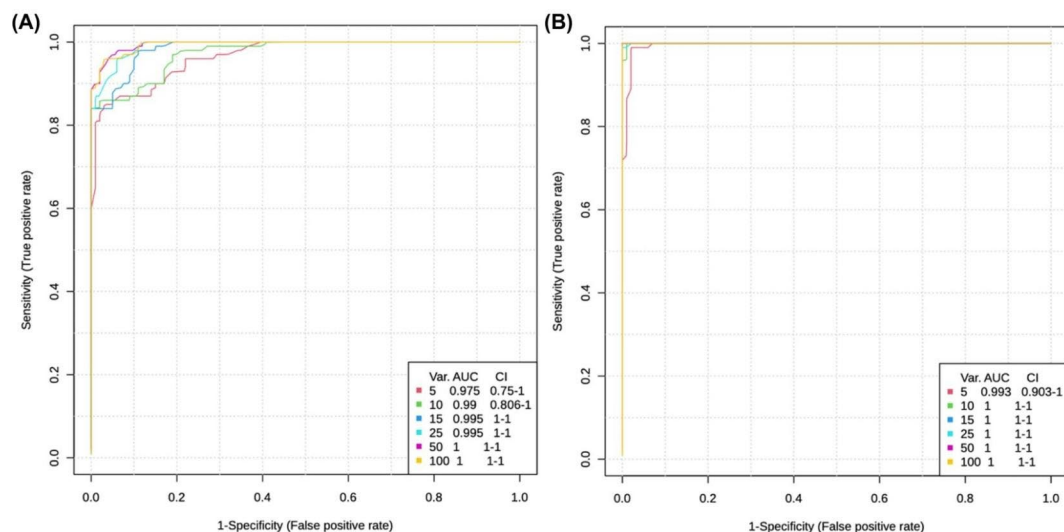


**Fig. 4.** Receiver Operating Characteristics (ROC) curve for significant metabolites. ROC was generated by the Random Forest model using MetaboAnalyst 6.0, employing different number of features (5, 10, 15, 25, 50 and 100). The corresponding Area Under the Curve (AUC) value and confidence interval (CI) were determined for each set of features. **(A)** ROC curves of the *cmybpc3*<sup>-/-</sup>::*myl7*:eGFP homozygous (HM) vs. control (CO) model. **(B)** ROC curves of the *cmybpc3*<sup>+/-</sup>::*myl7*:eGFP heterozygous (HT) vs. HM model.

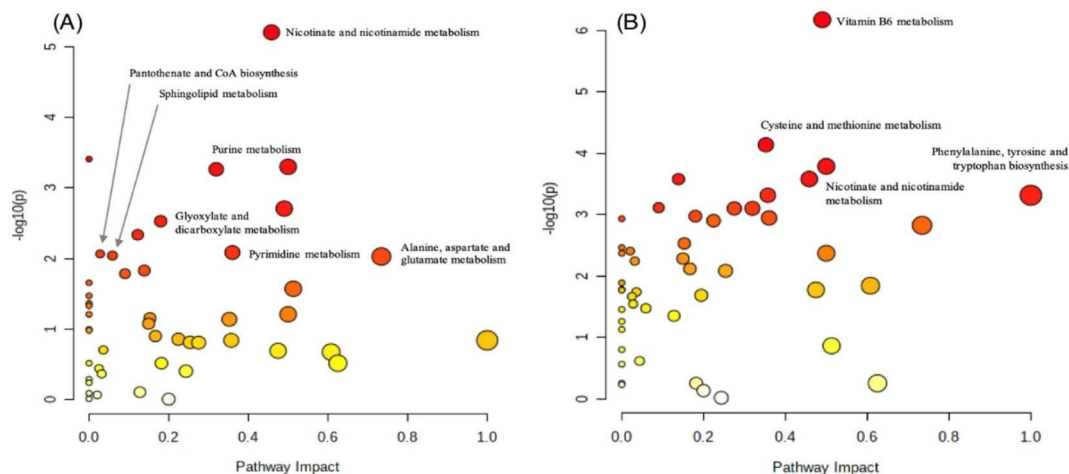


**Fig. 5.** Pathway enrichment analysis. Pathway enrichment analysis was done using MetaboAnalyst 5.0 and 6.0 using KEGG for species zebrafish (*Danio rerio*)<sup>63</sup>. The Y-axis shows the matched pathways according to the p-values from the pathway enrichment analysis and X-axis pathway impact values from the pathway topology analysis. The node color of each pathway is determined by the p-value (red = lowest p-value and highest statistical significance), and the node radius (size) is based on the pathway impact factor, with the biggest indicating the highest impact. Pathway enrichment analysis was done comparing **(A)** Homozygous and Control groups. **(B)** Homozygous and Heterozygous groups. Nicotinate and nicotinamide metabolism was significant in both Homozygous compared to Control and Heterozygous groups with p-values of 6.28E-6 and 2.65E-4, respectively.

This study revealed several significant differences in fatty acid, lipid and metabolite profiles detected in zebrafish homogenate samples between the examined CO, HT, and HM groups. The main alterations were seen with acylcarnitines, redox regulation via NAD/NADH, pyrimidine, and purine metabolism. These differences further prove the pathogenicity of *MYBPC3* genetic variation<sup>4,27,28</sup>.

The rate of acylcarnitine metabolism plays an essential role in maintaining a balance between lipid metabolism and levels of intracellular glucose<sup>29</sup>. Acylcarnitines function as activated long-chain fatty acid carriers, transporting fatty acids into the mitochondria for beta-oxidation, producing acetyl CoA, and subsequently providing cellular energy through the citric acid cycle<sup>30</sup>. As well, acylcarnitines have been associated with the

production of ketone bodies and the peroxidation of fatty acids<sup>31</sup>. Furthermore, acylcarnitines have been linked as potential biomarkers for HCM severity and other cardiovascular diseases<sup>27,32–34</sup>.

Fatty acids and associated lipids play an important role in cardiomyocyte structure and function<sup>35</sup>. Changes occur in fatty acids regulation during cardiac growth and development<sup>35</sup>. In HCM patients, reports of impaired myocardial fatty acid oxidation were identified through various multi-omics analyses<sup>28,36</sup>. This was linked to a decrease in acylcarnitine levels that affects the supply of efficient cellular energy in the heart<sup>4</sup>. Studies in patients with HCM have identified an inverse relationship between myocardial and circulating acylcarnitines levels<sup>37,38</sup>. In our zebrafish HCM model, a higher abundance of acylcarnitines was noted in HM group compared to HT and CO, suggesting higher use of beta-oxidation of fatty acids as an energy source. Moreover, plasma acylcarnitines were associated as one of the top metabolites that can draw the distinction between mild and severe forms of HCM in age and sex-matched patients<sup>39</sup>, highlighting the relevance of monitoring their levels in efficient HCM diagnosis.

Cardiac hypertrophy is induced by pressure overload with changes in fatty acids that were seen in our HM HCM model. The 9,12,15-octadecatrienoic acid, also known as alpha-linolenic acid (ALA), was highlighted as the highest VIP score distinguished among the three examined zebrafish groups with a higher level in HM and a lower level in HT compared to the control group. ALA is a polyunsaturated fatty acid that was found to play a crucial role as a structural component in cell membranes, affecting permeability, flexibility and fluidity along with other omega-3 fatty acid<sup>40</sup>. Also, these fatty acids have been shown to have highly protective effects in cardiovascular disease-associated risks by suppressing pro-inflammatory cytokines<sup>41–43</sup>.

In regard to saturated fatty acids, our analysis demonstrated that hexadecenoic (palmitic acid) was highlighted as the second highest VIP score fatty acids distinguishing the examined profiles. Long fatty acid chains, such as palmitic acid and S-59-adenosyl-methionine through the catechol-O-methyltransferase biosynthesize palmitic acid methyl ester, have been shown earlier to activate voltage-dependent  $Ca^{2+}$  channels that are associated with HCM<sup>44–46</sup>.

The fatty acid levels showed opposite trends in our zebrafish model, with higher levels in HM group and lower levels in HT group in comparison to the control group. This might be due to the fact that HT group resembles the human autosomal dominant HCM disease, while truncating variants were reported to be lethal<sup>47</sup>. Cardiomyocytes generate two-thirds of ATP by the oxidation of fatty acids and one-third by glucose<sup>48</sup>. In end-stage heart failure patients, a decrease in fatty acid oxidation and a shift towards increased glucose metabolism leading to fatty acids accumulation was reported<sup>49,50</sup>, where as in our zebrafish HM group, a similar signature was observed. In contrast, our results suggest that the HT group fatty acid levels appear to be compensating for energy demands through the oxidation of fatty acids.

Importantly, oxidative stress is implicated in various cardiac diseases, including HCM and heart failure. It plays a key role in HCM remodeling and dysfunction<sup>51</sup>. The initiation of HCM occurs via the  $Ca^{2+}$ -dependent pathway, activated by mitochondrial reactive oxygen species (ROS), triggering the cardiac  $Na^+/Ca^{2+}$  exchanger<sup>52,53</sup>. Additionally, serum biomarkers indicative of oxidative stress were observed in patients with HCM<sup>51</sup>. Similar to previous findings, metabolic pathways associated with oxidative stress were significantly dysregulated in our zebrafish *cmybpc3*<sup>-/-</sup> HM compared to *cmybpc3*<sup>+/-</sup> HT group. Methionine, S-adenosylmethionine and cysteine were significantly dysregulated in the HM, suggesting an imbalance between the production of ROS and the ability to detoxify them within the model.

Notably, nicotinate, nicotinamide and tryptophan metabolites were upregulated in *cmybpc3*<sup>-/-</sup> HM compared to CO and HT groups. NAD<sup>+</sup> is involved in many metabolic processes, including energy metabolism and stress response, in which significant pathophysiological alterations have been observed in HCM patients<sup>54,55</sup>. NAD<sup>+</sup> can be synthesized either through the *de novo* pathway using tryptophan or through the salvage pathway using nicotinamide riboside, nicotinamide mononucleotide, nicotinic acid, nicotinamide, or nicotinamide ribose. Our observation is consistent with earlier studies that reported a depletion of cellular NAD<sup>+</sup> levels in HCM models and patients, suggesting an increased effort to synthesize more NAD<sup>+</sup> in response to severe oxidative stress<sup>56–58</sup>.

Furthermore, we identified disruptions in pathways involving purines, pyrimidines, and glycerophospholipids, comparing the HM to CO zebrafish groups. Consistent with previous reports of HCM models and patients' data<sup>37,59,60</sup>, a link between purine and pyrimidine metabolite alterations was demonstrated in our zebrafish model. In addition, according to the New York Heart Association categorization, a significant relationship was identified between purine and pyrimidine metabolites indicative of a worse prognosis in HCM patients<sup>16</sup>. As well, HCM patients' lipidomics analysis showed altered levels of glycerophospholipids and triglycerides<sup>60</sup>.

The present study, while providing valuable insights into cardiac remodeling in HCM model, is not without its limitations. While the zebrafish model is advantageous for its genetic tractability and experimental manipulability, caution must be exercised when extrapolating findings to the complexities of the human cardiovascular system. One notable limitation pertains to the intrinsic anatomical disparity between the zebrafish heart, with its two-chambered structure, and the human heart, which is characterized by a more complex four-chambered configuration. Additionally, using laboratory animal models, while beneficial for controlled experimental conditions, introduces some limitations related to these optimal conditions. The multifactorial nature of cardiovascular health, influenced by lifestyle, dietary habits, and environmental factors, is inherently challenging to fully replicate in a controlled laboratory setting. Furthermore, we utilized whole larvae lysate samples as the process of dissecting the zebrafish hearts while preserving sample integrity poses a technical challenge that could impact the reliability of results. To address this, we opted to analyze the entire zebrafish lysate, believing this approach may unveil unique and significant differences in metabolomics and lipidomics profiles, providing a comprehensive perspective on cardiac physiology in this model organism. Overall, while this study provides valuable insights into the metabolic perturbations underlying HCM, addressing these limitations for future research directions will not only enhance our understanding of HCM but also pave the

way for developing more effective therapeutic interventions. This potential impact should instill hope in the future of HCM research and treatment.

In conclusion, our study provides a comprehensive multi-omics assessment of hypertrophic cardiomyopathy (HCM) using the *cmybpc3*<sup>-/-</sup> zebrafish model, highlighting significant alterations in lipidomic and metabolomic profiles associated with the disease. The findings underscore the importance of acylcarnitines, phosphatidylcholines, and various metabolic pathways, including nicotine, nicotinate, nicotine, purine, pyrimidine, and amino acid metabolism, in HCM pathophysiology. These findings are significant and should be a cornerstone for future research in this field.

Future research should investigate the mechanistic roles of these identified metabolites and lipids in HCM progression, validate our findings in mammalian models, and conduct longitudinal studies to monitor changes over time. Additionally, exploring the dysregulated pathways as potential therapeutic targets and developing drug models to test in zebrafish and other systems could offer new treatment strategies.

## Materials and methods

### Zebrafish care and maintenance

Zebrafish (*Danio rerio*) Tg *myl7:eGFP* line as a control (CO), *cmybpc3*<sup>+/-</sup>::*myl7:eGFP* heterozygous (HT) and *cmybpc3*<sup>-/-</sup>::*myl7:eGFP* homozygous (HM) adults were maintained in standard conditions according to the Ministry of Public Health (MOPH), Qatar animal research guidelines and under an approved protocol by the Institutional Animal Care Committee (Qatar Foundation, protocol IACUC 2020–1132) and adhered to the ARRIVE guidelines. The adult zebrafish were setup for breeding, the embryos were collected and incubated in E3 egg water media (5.0mM NaCl, 0.17mM KCl, 0.16mM MgSO<sub>4</sub>·7H<sub>2</sub>O, 0.4mM CaCl<sub>2</sub>·2H<sub>2</sub>O in ddH<sub>2</sub>O) at 28.5 °C.

### Zebrafish sample lysis

For each experimental group, CO, HT, and HM at 5 days old, 150 larvae were pooled in one tube with a total of 7 replicates for each group to obtain more information on fatty acids, metabolomic and lipidomic profiles. All deformed larvae were excluded prior to collection; no criteria were set for exclusion during the experiment. Excess media in the pooled larvae tubes was removed, then the tubes were snap frozen in liquid nitrogen then stored in -80 °C freezer until further processing. All samples were processed as previously described<sup>61</sup> with some modifications; the samples were homogenized in chilled 400 µL methanol (Fisher A456-500) using a Bell-Art pestle tube homogenizer (SCIENCEWARE F19923-0000), and kept on ice for 20 min; then vortexed at 2000 rpm, 4 °C for three cycles of 10 s with a 15 s break between each cycle using an Eppendorf thermomixer. Then, it was centrifuged at 14,000 g for 5 min at 4 °C, and 400 µL of the supernatant was collected in glass vials (Waters 186007201 C). The supernatant was further processed and analyzed by three methods for fatty acid profiling, metabolomics and lipidomics. The different groups were de-identified throughout analysis.

### Fatty acid methyl ester analysis

Fatty acid analysis was conducted on 50 µL of the zebrafish homogenate supernatant after converting total lipids to fatty acid methyl esters through transesterification. The samples were transferred to 10 mL Reacti-vial vials (Thermo Scientific TS13225) and 2 mL of 25mL/L H<sub>2</sub>SO<sub>4</sub> (Sigma Aldrich 339741) in methanol was added. The mixture was mixed and then placed in an oven for 2 h at 60 °C. Once the tubes were cooled at room temperature, 2 mL of saturated NaCl (Sigma Aldrich 31434) in H<sub>2</sub>O was added and mixed, followed by 1 mL of hexane (Scharlau HE02342500). Following centrifugation, the hexane layer was transferred to a glass vial and any trace amounts of water were removed by mixing a small amount of Na<sub>2</sub>SO<sub>4</sub> (Sigma Aldrich 798592) to the solution. The sample was then transferred to an autosampler vial and injected into a gas chromatograph coupled to a single quadrupole mass spectrometer in Scan mode (Agilent Technologies, Santa Clara, CA).

GC-MS analyses were carried out on an Agilent 7890 C gas chromatograph with a 5977 A EI-MSD (Agilent Technologies, Wilmington, DE). Chromatography was carried out using a 60 m x 0.25 mm TR-FAME capillary column with a film thickness of 0.25 µm (Thermo Scientific, Waltham, MA). Helium was used as the carrier gas at a flow rate of 1.0 mL/min with constant flow compensation. The GC inlet were held at 290 °C, and the MS transfer line was maintained at 260 °C. Sample injections of 0.5 µL were performed with a split ratio of 5:1. After a solvent delay of 8.7 min, the oven temperature was programmed from 30 to 200 °C at a rate of 5 °C/min and then to 220 °C at 1 °C/min and to 260 °C at 6.5 °C/min with a final hold of 2 min. Full-scan acquisition with electron impact ionization carried out using 70 eV was used for quantification based on the extracted ion chromatogram. All mass spectra were acquired over the m/z range of 30–500. Spectra were matched with a FAME standard mix (37 Component FAME Mix, Supelco, Whippany, NJ) or putatively annotated by comparison with NIST EI library (2017 release).

### Metabolomics analysis

An aliquot of the zebrafish homogenate supernatant (125 µL) was transferred to glass vials and 20 µL of isotopically labelled QC standard mix (MSK-QC-KIT, Metabolomics QC Kit, Cambridge Isotope Laboratories, Tewsbury, MA) was added. The mixture was evaporated in a vacuum centrifuge (Genevac EZ-2 Plus, Genevac Ltd, Ipswich, UK) to dryness. The residue was then stored in -80 °C freezer until analysis. After reconstitution in 90 µL of 1% methanol in water (Fisher W6500), 20 µL of each sample was mixed to prepare a sample mix used for compound identification. Each sample was injected individually (2 µL injection volume) on an ultra-high pressure liquid chromatograph coupled to an orbitrap tribrid mass spectrometer (Vanquish LC and Fusion Lumos, Thermo Scientific, Waltham, MA). The column utilized was an Accucore C18+ reverse phase column (27101–152130, 2.1 × 150 mm, 1.5 µm, Thermo Scientific, Waltham, MA) held at 45 °C and using a mobile phase gradient of H<sub>2</sub>O and methanol with 0.1% formic acid (Fisher A1171-AMP) additive (MPA and MPB respectively) at a flow



rate of 0.2 mL/min. Initial mobile phase conditions were 1% MPB rising to 100% MPB over 12 min. The heated electrospray ion source (NGS-HESI) was operated with a sheath gas flow of 40 AU, auxiliary gas flow rate of 8 AU, sweep gas flow of 1 AU and spray voltage of 3.5 kV or 3 kV in positive and negative mode respectively. The vaporizer and ion transfer tube temperature settings were 320 °C and 275 °C respectively. Automatic gain control target was set to 1E5 ions and with an auto setting of maximum injection time and RF lens setting of 35%. Each sample was injected four times with varied method parameters: (1) positive ESI polarity with low mass range (59–250  $m/z$ ), (2) positive ESI polarity with high mass range (250–1200  $m/z$ ), (3) negative ESI polarity with low mass range, and (4) negative ESI polarity with high mass range, all in full scan mode with orbitrap mass resolution of 240 K (FWHM at  $m/z$  200) with internal calibration of all scans with fluoranthene ion. The sample mix was injected numerous times with AcquireX deep scan mode to enable maximal MS2 fragmentation with HCD fragmentation mode of detected peaks above an intensity threshold of 2E4. The data-dependent MS/MS mode utilized an orbitrap mass resolution of 60 K in MS1 and 30 K in MS2 and stepped collision energies of 20, 35 and 50%. Dynamic exclusion was utilized with isotope exclusion and feature exclusion for 4 s after one MS2 scan with a mass tolerance setting of 3ppm.

### Lipidomics analysis

Another aliquot of the zebrafish homogenate supernatant (125  $\mu$ L) was transferred to glass vials and 20  $\mu$ L of isotopically labelled lipid QC mix (330707, Splash Lipidomix, Avanti Polar Lipids, Alabaster, AL) and 805  $\mu$ L of H<sub>2</sub>O: CHCl<sub>3</sub>:methanol (24.8:31.1:44.1) was added and the mixture mixed. Another 250  $\mu$ L of CHCl<sub>3</sub> was then added and the mixture was mixed, followed by an aliquot of 250  $\mu$ L of H<sub>2</sub>O and mixing. The mixture was centrifuged at 4000 rpm at 15 °C for 15 min to produce a bilayer. The bottom layer (400  $\mu$ L) was transferred to a glass vial and evaporated in a vacuum centrifuge and the residue stored at –80 °C until analysis. On the day of analysis, the sample was reconstituted in 100  $\mu$ L of isopropanol: methanol: CHCl<sub>3</sub> (1:1:1, isopropanol Fisher IA461-500, CHCl<sub>3</sub> Sigma Aldrich 650498) and 20  $\mu$ L of each sample mixed to make a sample mix. Each sample (1  $\mu$ L injection volume) was injected as above with a column temperature setting of 70 °C using mobile phases acetonitrile: water (6:4, MPA) and acetonitrile: isopropanol (1:9, MPB), each with 0.1% formic acid and 10 mM ammonium acetate as additives. The initial mobile phase condition was 10% MPB and rose to 100% over 32 min. The HESI source was set to sheath gas flow 40 AU, auxiliary gas flow 7 AU, sweep gas flow 1 AU and spray voltages 3.5 kV and 2.8 kV in positive and negative modes, respectively, with vaporizer temperature of 300 °C and ion transfer tube temperature 350 °C. Automatic gain control target was set to 2E5 ions, with an auto setting of maximum injection time and RF lens setting of 60%. Each sample was injected twice in ESI positive and negative scan mode at 240 K orbitrap mass resolution with a full scan mass range of 200–2000  $m/z$ . The sample mix was injected several times with AcquireX deep scan mode to enable MS2 fragmentation in HCD fragmentation mode utilizing an orbitrap mass resolution of 120 K in MS1 and 15 K in MS2 with stepped collision energies of 25, 30 and 35% and a method that triggered CID fragmentation at 32% and 35% collision energies after the detection of the phosphocholine headgroup ( $m/z$  184.0733) and the fragment ions formed by the neutral loss of M + NH<sub>4</sub> adducts of common fatty acids respectively.

### Data processing and analysis

The processing of data files was conducted using Compound Discoverer (version 3.3), where features were aligned and grouped with a mass tolerance of 3 and 5 ppm for metabolomics and lipidomics samples, respectively, with a retention time maximum shift of 0.2 min. Lipidomics samples were annotated with LipidSearch (version 4.23), allowing for [M + H]<sup>+</sup>, [M + NH<sub>4</sub>]<sup>+</sup>, [M + Na]<sup>+</sup>, [M + H-H<sub>2</sub>O]<sup>+</sup>, [M-H]<sup>-</sup>, [M + HCOO]<sup>-</sup> and [M + CH<sub>3</sub>COO]<sup>-</sup> ions with a mass tolerance of 5 ppm and fragment mass tolerance of 10 ppm. Features in the metabolomics data files were annotated with the following online databases: (1) in-house MS2 library of over 950 metabolite compounds where match factors were elemental composition, retention time and MS2 spectrum and (2) mzCloud where match factors were elemental composition and MS2 spectrum, both with a parent mass tolerance of 5 ppm and fragment mass tolerance of 10 ppm. All discovered compounds were integrated for peak area in each sample and used for statistical analysis.

The added isotopically-labeled internal standards were monitored in each sample for retention time fluctuations, peak abundance and mass accuracy. The monitored peaks were within acceptable limits of  $\pm$  2% of median retention time,  $\pm$  30% of median peak abundance and  $\pm$  3 ppm mass accuracy.

MetaboAnalyst v5.0 and v6.0<sup>62</sup>Superscript> were used for multivariate statistics. Log10 data transformation and Pareto scaling were applied to all data. Initially, the variance in the data was analysed using Principal Components Analysis (PCA). Following this, a Partial Least Squares - Discriminant Analysis (PLS-DA) was applied and variable importance was assessed using VIP (variable importance in projection) scores. Sparse PLS-DA was used for metabolomics and lipidomics data to effectively reduce the number of variables. In this analysis, five components were used with 10 variables per component. Hierarchical clustering heatmaps were generated using Euclidean distance measure and Ward clustering method. Pathway enrichment analysis was performed with global Ancova with topology analysis set to relative-betweenness centrality. ROC curve analysis was performed using Random Forests with Monte-Carlo cross-validation where within each iteration, the data was split randomly into two-thirds training and one-third validation sets. This multivariate study on lab-grown zebrafish in a highly controlled environment where comparisons were made with an experimental control group has minimal confounders.

### Data availability

All data generated or analysed during this study are included in this published article and its supplementary information files.

Received: 21 February 2024; Accepted: 11 September 2024

Published online: 19 September 2024

## References

- Antunes, M. O. & Scudeler, T. L. Hypertrophic cardiomyopathy. *Int. J. Cardiol. Heart Vasc.* **27**, 100503. <https://doi.org/10.1016/j.ijcha.2020.100503> (2020).
- Marian, A. J., Braunwald, E. & Hypertrophic Cardiomyopathy Genetics, Pathogenesis, clinical manifestations, diagnosis, and Therapy. *Circ. Res.* **121**, 749–770. <https://doi.org/10.1161/circresaha.117.311059> (2017).
- Maron, B. J. et al. Diagnosis and evaluation of hypertrophic cardiomyopathy: JACC state-of-the-art review. *J. Am. Coll. Cardiol.* **79**, 372–389. <https://doi.org/10.1016/j.jacc.2021.12.002> (2022).
- Ranjbarvaziri, S. et al. Altered Cardiac energetics and mitochondrial dysfunction in hypertrophic cardiomyopathy. *Circulation.* **144**, 1714–1731. <https://doi.org/10.1161/circulationaha.121.053575> (2021).
- Hong, Y., Su, W. W. & Li, X. Risk factors of sudden cardiac death in hypertrophic cardiomyopathy. *Curr. Opin. Cardiol.* **37**, 15–21. <https://doi.org/10.1097/hco.0000000000000939> (2022).
- Akhtar, M. & Elliott, P. The genetics of hypertrophic cardiomyopathy. *Glob. Cardiol. Sci. Pract.* **36**, doi: (2018). <https://doi.org/10.21542/gcsp.2018.36> (2018).
- Glavaški, M., Velicki, L. & Vučinić, N. Hypertrophic cardiomyopathy: genetic foundations, outcomes, interconnections, and their modifiers. *Med. (Kaunas)*. **59** <https://doi.org/10.3390/medicina59081424> (2023).
- Park, J. et al. A genome-first approach to rare variants in hypertrophic cardiomyopathy genes MYBPC3 and MYH7 in a medical biobank. *Hum. Mol. Genet.* **31**, 827–837. <https://doi.org/10.1093/hmg/ddab249> (2022).
- Tran Vu, M. T. et al. Presence of Hypertrophic Cardiomyopathy related gene mutations and clinical manifestations in Vietnamese patients with hypertrophic cardiomyopathy. *Circ. J.* **83**, 1908–1916. <https://doi.org/10.1253/circj.CJ-19-0190> (2019).
- Velicki, L. et al. Genetic determinants of clinical phenotype in hypertrophic cardiomyopathy. *BMC Cardiovasc. Disord.* **20**, 516. <https://doi.org/10.1186/s12872-020-01807-4> (2020).
- Liu, X. et al. Screening mutations of MYBPC3 in 114 unrelated patients with hypertrophic cardiomyopathy by targeted capture and next-generation sequencing. *Sci. Rep.* **5**, 11411. <https://doi.org/10.1038/srep11411> (2015).
- Helms, A. S. et al. Spatial and functional distribution of MYBPC3 pathogenic variants and clinical outcomes in patients with hypertrophic cardiomyopathy. *Circ. Genom. Precis. Med.* **13**, 396–405. <https://doi.org/10.1161/circgen.120.002929> (2020).
- Previs, M. J., Previs, S. B., Gulick, J., Robbins, J. & Warshaw, D. M. Molecular mechanics of Cardiac myosin-binding protein C in native thick filaments. *Science*. **337**, 1215–1218. <https://doi.org/10.1126/science.1223602> (2012).
- Suay-Corredera, C. & Alegre-Cebollada, J. The mechanics of the heart: zooming in on hypertrophic cardiomyopathy and cMyBP-C. *FEBS Lett.* **596**, 703–746. <https://doi.org/10.1002/1873-3468.14301> (2022).
- Glazier, A. A., Thompson, A. & Day, S. M. Allelic imbalance and haploinsufficiency in MYBPC3-linked hypertrophic cardiomyopathy. *Pflugers Arch.* **471**, 781–793. <https://doi.org/10.1007/s00424-018-2226-9> (2019).
- Wang, W. et al. Metabolic characterization of hypertrophic cardiomyopathy in human heart. *Nat. Cardiovasc. Res.* **1**, 445–461. <https://doi.org/10.1038/s44161-022-00057-1> (2022).
- Maurizi, N. et al. Clinical course and significance of hypertrophic cardiomyopathy without left ventricular hypertrophy. *Circulation.* **139**, 830–833. <https://doi.org/10.1161/circulationaha.118.037264> (2019).
- Ingles, J. et al. Nonfamilial hypertrophic cardiomyopathy. *Circulation: Cardiovasc. Genet.* **10**, e001620. <https://doi.org/10.1161/CIRCGENETICS.116.001620> (2017).
- Sequeira, V., Bertero, E. & Maack, C. Energetic drain driving hypertrophic cardiomyopathy. *FEBS Lett.* **593**, 1616–1626. <https://doi.org/10.1002/1873-3468.13496> (2019).
- Doenst, T., Nguyen, T. D. & Abel, E. D. Cardiac metabolism in heart failure: implications beyond ATP production. *Circ. Res.* **113**, 709–724. <https://doi.org/10.1161/circresaha.113.300376> (2013).
- Seth, A., Stemple, D. L. & Barroso, I. The emerging use of zebrafish to model metabolic disease. *Dis. Model. Mech.* **6**, 1080–1088. <https://doi.org/10.1242/dmm.011346> (2013).
- Xu, M., Legradi, J. & Leonards, P. A comprehensive untargeted metabolomics study in zebrafish embryos exposed to perfluorohexane sulfonate (PFHxS). *Sci. Total Environ.* **887**, 163770. <https://doi.org/10.1016/j.scitotenv.2023.163770> (2023).
- Daás, S. I. et al. Hypertrophic cardiomyopathy-linked variants of cardiac myosin-binding protein C3 display altered molecular properties and actin interaction. *Biochem. J.* **475**, 3933–3948. <https://doi.org/10.1042/bcj20180685> (2018).
- Daás, S. I. et al. Functional characterization of human myosin-binding protein C3 variants associated with hypertrophic cardiomyopathy reveals exon-specific cardiac phenotypes in zebrafish model. *J. Cell. Physiol.* **235**, 7870–7888. <https://doi.org/10.1002/jcp.29441> (2020).
- Daás, S. I. et al. Transcriptome Profile identifies actin as an essential Regulator of Cardiac myosin binding protein C3 hypertrophic cardiomyopathy in a zebrafish model. *Int. J. Mol. Sci.* **23**, 8840 (2022).
- Elfatih, A. et al. Analysis of incidental findings in Qatar genome participants reveals novel functional variants in LMNA and DSP. *Hum. Mol. Genet.* **31**, 2796–2809. <https://doi.org/10.1093/hmg/ddac073> (2022).
- Jansen, M. et al. Untargeted Metabolomics identifies potential hypertrophic cardiomyopathy biomarkers in carriers of MYBPC3 founder variants. *Int. J. Mol. Sci.* **24** <https://doi.org/10.3390/ijms24044031> (2023).
- Pei, J. et al. Multi-omics integration identifies key upstream regulators of pathomechanisms in hypertrophic cardiomyopathy due to truncating MYBPC3 mutations. *Clin. Epigenetics.* **13**, 61. <https://doi.org/10.1186/s13148-021-01043-3> (2021).
- Qu, Q., Zeng, F., Liu, X., Wang, Q. J. & Deng, F. Fatty acid oxidation and carnitine palmitoyltransferase I: emerging therapeutic targets in cancer. *Cell. Death Dis.* **7**, e2226. <https://doi.org/10.1038/cddis.2016.132> (2016).
- Tarasenko, T. N., Cusmano-Ozog, K. & McGuire, P. J. Tissue acylcarnitine status in a mouse model of mitochondrial  $\beta$ -oxidation deficiency during metabolic decompensation due to influenza virus infection. *Mol. Genet. Metab.* **125**, 144–152. <https://doi.org/10.1016/j.ymgme.2018.06.012> (2018).
- Xiang, L. et al. Comprehensive Analysis of Acylcarnitine Species in db/db mouse using a novel method of high-resolution parallel reaction monitoring reveals widespread metabolic Dysfunction Induced by Diabetes. *Anal. Chem.* **89**, 10368–10375. <https://doi.org/10.1021/acs.analchem.7b02283> (2017).
- Aitken-Buck, H. M., Krause, J., Zeller, T., Jones, P. P. & Lamberts, R. R. Long-chain acylcarnitines and Cardiac Excitation-Contraction Coupling: links to Arrhythmias. *Front. Physiol.* **11**, 577856. <https://doi.org/10.3389/fphys.2020.577856> (2020).
- Deda, O. et al. Correlation of serum acylcarnitines with clinical presentation and severity of coronary artery disease. *Biomolecules.* **12** <https://doi.org/10.3390/biom12030354> (2022).
- Shah, S. H., Kraus, W. E. & Newgard, C. B. Metabolomic profiling for the identification of novel biomarkers and mechanisms related to common cardiovascular diseases: form and function. *Circulation.* **126**, 1110–1120. <https://doi.org/10.1161/circulationaha.111.060368> (2012).
- Yang, X. et al. Fatty acids enhance the maturation of Cardiomyocytes Derived from Human pluripotent stem cells. *Stem Cell. Rep.* **13**, 657–668. <https://doi.org/10.1016/j.stemcr.2019.08.013> (2019).
- Previs, M. J. et al. Defects in the Proteome and Metabolome in Human hypertrophic cardiomyopathy. *Circ. Heart Fail.* **15**, e009521. <https://doi.org/10.1161/circheartfailure.121.009521> (2022).

37. Schuldt, M. et al. Distinct metabolomic signatures in preclinical and obstructive hypertrophic cardiomyopathy. *Cells*. **10**<https://doi.org/10.3390/cells10112950> (2021).
38. Shimada, Y. J. et al. Difference in Metabolomic Response to Exercise between patients with and without Hypertrophic Cardiomyopathy. *J. Cardiovasc. Transl. Res.* **14**, 246–255. <https://doi.org/10.1007/s12265-020-10051-2> (2021).
39. Jansen, M. et al. Circulating Acylcarnitines Associated with hypertrophic cardiomyopathy severity: an exploratory cross-sectional study in MYBPC3 founder variant carriers. *J. Cardiovasc. Transl. Res.* <https://doi.org/10.1007/s12265-023-10398-2> (2023).
40. Wishart, D. S. et al. HMDB 5.0: the human metabolome database for 2022. *Nucleic Acids Res.* **50**, D622–d631. <https://doi.org/10.1093/nar/gkab1062> (2022).
41. Duda, M. K., O’Shea, K. M. & Stanley, W. C. omega-3 polyunsaturated fatty acid supplementation for the treatment of heart failure: mechanisms and clinical potential. *Cardiovasc. Res.* **84**, 33–41. <https://doi.org/10.1093/cvr/cvp169> (2009).
42. Kris-Etherton, P. M., Harris, W. S. & Appel, L. J. Fish consumption, fish oil, omega-3 fatty acids, and cardiovascular disease. *Circulation*. **106**, 2747–2757. <https://doi.org/10.1161/01.cir.0000038493.65177.94> (2002).
43. Toko, H. et al. Omega-3 fatty acid prevents the development of heart failure by changing fatty acid composition in the heart. *Sci. Rep.* **10**, 15553. <https://doi.org/10.1038/s41598-020-72686-0> (2020).
44. Bendahhou, S., Cummins, T. R. & Agnew, W. S. Mechanism of modulation of the voltage-gated skeletal and cardiac muscle sodium channels by fatty acids. *Am. J. Physiol.* **272**, C592–600. <https://doi.org/10.1152/ajpcell.1997.272.2.C592> (1997).
45. Huang, J. M., Xian, H. & Bacaner, M. Long-chain fatty acids activate calcium channels in ventricular myocytes. *Proc. Natl. Acad. Sci. U S A*. **89**, 6452–6456. <https://doi.org/10.1073/pnas.89.14.6452> (1992).
46. Lien, C. F. et al. Palmitic acid methyl ester induces cardiac hypertrophy through activating the GPR receptor-mediated changes of intracellular calcium concentrations and mitochondrial functions. *J. Cell. Physiol.* **238**, 242–256. <https://doi.org/10.1002/jcp.30922> (2023).
47. Wessels, M. W. et al. Compound heterozygous or homozygous truncating MYBPC3 mutations cause lethal cardiomyopathy with features of noncompaction and septal defects. *Eur. J. Hum. Genet.* **23**, 922–928. <https://doi.org/10.1038/ejhg.2014.211> (2015).
48. van der Velden, J. et al. Metabolic changes in hypertrophic cardiomyopathies: scientific update from the Working Group of myocardial function of the European Society of Cardiology. *Cardiovasc. Res.* **114**, 1273–1280. <https://doi.org/10.1093/cvr/cvy147> (2018).
49. Lionetti, V., Stanley, W. C. & Recchia, F. A. Modulating fatty acid oxidation in heart failure. *Cardiovasc. Res.* **90**, 202–209. <https://doi.org/10.1093/cvr/cvr038> (2011).
50. Sharma, S. et al. Intramyocardial lipid accumulation in the failing human heart resembles the lipotoxic rat heart. *Faseb j.* **18**, 1692–1700. <https://doi.org/10.1096/fj.04-2263com> (2004).
51. Rababa’h, A. M., Guillory, A. N., Mustafa, R. & Hijjawi, T. Oxidative stress and Cardiac Remodeling: an updated edge. *Curr. Cardiol. Rev.* **14**, 53–59. <https://doi.org/10.2174/1573403x1466618011145207> (2018).
52. Cingolani, H. E. et al. Early signals after stretch leading to cardiac hypertrophy. Key role of NHE-1. *Front. Biosci.* **13**, 7096–7114. <https://doi.org/10.2741/3213> (2008).
53. Palomeque, J. et al. Angiotensin II-induced oxidative stress resets the Ca<sup>2+</sup> dependence of Ca<sup>2+</sup>-calmodulin protein kinase II and promotes a death pathway conserved across different species. *Circ. Res.* **105**, 1204–1212. <https://doi.org/10.1161/circresaha.109.204172> (2009).
54. Sultani, G., Samsudeen, A. F., Osborne, B. & Turner, N. NAD(+): a key metabolic regulator with great therapeutic potential. *J. Neuroendocrinol.* **29** <https://doi.org/10.1111/jne.12508> (2017).
55. Zhang, X., Zhang, Y., Sun, A. & Ge, J. The effects of nicotinamide adenine dinucleotide in cardiovascular diseases: molecular mechanisms, roles and therapeutic potential. *Genes Dis.* **9**, 959–972. <https://doi.org/10.1016/j.gendis.2021.04.001> (2022).
56. Pillai, J. B., Isbatan, A., Imai, S. & Gupta, M. P. Poly(ADP-ribose) polymerase-1-dependent cardiac myocyte cell death during heart failure is mediated by NAD<sup>+</sup> depletion and reduced Sir2alpha deacetylase activity. *J. Biol. Chem.* **280**, 43121–43130. <https://doi.org/10.1074/jbc.M506162200> (2005).
57. Pillai, V. B. et al. Exogenous NAD blocks cardiac hypertrophic response via activation of the SIRT3-LKB1-AMP-activated kinase pathway. *J. Biol. Chem.* **285**, 3133–3144. <https://doi.org/10.1074/jbc.M109.077271> (2010).
58. Schuldt, M. et al. Proteomic and functional studies reveal deetyrosinated tubulin as treatment target in Sarcomere Mutation-Induced Hypertrophic Cardiomyopathy. *Circ. Heart Fail.* **14**, e007022. <https://doi.org/10.1161/circheartfailure.120.007022> (2021).
59. Ritterhoff, J. et al. Metabolic remodeling promotes Cardiac Hypertrophy by directing glucose to Aspartate Biosynthesis. *Circ. Res.* **126**, 182–196. <https://doi.org/10.1161/circresaha.119.315483> (2020).
60. Wang, Y. et al. Lipidomics Changes in a murine model of neuropsychiatric lupus. *J. Inflamm. Res.* **15**, 6569–6580. <https://doi.org/10.2147/jir.S391595> (2022).
61. Xu, M., Legradi, J. & Leonards, P. Cross platform solutions to improve the zebrafish polar metabolome coverage using LC-QTOF MS: optimization of separation mechanisms, solvent additives, and resuspension solvents. *Talanta*. **234**, 122688. <https://doi.org/10.1016/j.talanta.2021.122688> (2021).
62. Pang, Z. et al. MetaboAnalyst 5.0: narrowing the gap between raw spectra and functional insights. *Nucleic Acids Res.* **49**, W388–w396. <https://doi.org/10.1093/nar/gkab382> (2021).
63. Kanehisa, M. & Goto, S. KEGG: kyoto encyclopedia of genes and genomes. *Nucleic Acids Res.* **28**, 27–30 (2000).

## Acknowledgements

We acknowledge Sidra Medicine – Research Department for funding support, R & D Budget for Zebrafish Functional Genomics Core Facility. We also acknowledge Dean Markus Wenk’s, College of Health and Life Sciences, Hamad Bin Khalifa University, Qatar, review of the article.

## Author contributions

SJ performed metabolomics, lipidomics sample analysis and generated profiles and figures; TA and RS contributed significantly to manuscript writing; AH, DA, HA, and KA provided technical support for zebrafish care and maintenance; WH and SB performed sample collection and processing; MN, KF, and ME contributed to the research design and conceptualization; SID performed project management, conceptualization, design, analysis and manuscript writing. All authors reviewed and approved the final version of the manuscript.

## Funding

We acknowledge Sidra Medicine – Research Department for funding support, R & D Budget for Zebrafish Functional Genomics Core Facility.

## Competing interests

The authors declare no competing interests.

### **Ethics declaration and consent to participate**

Zebrafish were maintained in standard conditions according to the Ministry of Public Health (MOPH), Qatar animal research guidelines and under an approved protocol by the Institutional Animal Care Committee (Qatar Foundation, protocol IACUC 2020 – 1132). Renewal approval: 1st of June 2023-1st of June 2026. This study follows the ARRIVE Guidelines.

### **Additional information**

**Supplementary Information** The online version contains supplementary material available at <https://doi.org/10.1038/s41598-024-72863-5>.

**Correspondence** and requests for materials should be addressed to S.I.D.

**Reprints and permissions information** is available at [www.nature.com/reprints](http://www.nature.com/reprints).

**Publisher's note** Springer Nature remains neutral with regard to jurisdictional claims in published maps and institutional affiliations.

**Open Access** This article is licensed under a Creative Commons Attribution-NonCommercial-NoDerivatives 4.0 International License, which permits any non-commercial use, sharing, distribution and reproduction in any medium or format, as long as you give appropriate credit to the original author(s) and the source, provide a link to the Creative Commons licence, and indicate if you modified the licensed material. You do not have permission under this licence to share adapted material derived from this article or parts of it. The images or other third party material in this article are included in the article's Creative Commons licence, unless indicated otherwise in a credit line to the material. If material is not included in the article's Creative Commons licence and your intended use is not permitted by statutory regulation or exceeds the permitted use, you will need to obtain permission directly from the copyright holder. To view a copy of this licence, visit <http://creativecommons.org/licenses/by-nc-nd/4.0/>.

© The Author(s) 2024